International Symposium
On Turbulence and Shear Flow
Phenomena (TSFP-8)
August 28 - 30, 2013 Poitiers, France

DNS OF A TRANSITIONALLY ROUGH CHANNEL FLOW WITH A 3-D ROUGHNESS

M. Seddighi[1], S. He[1], A. E. Vardy[2], T. O'Donoghue[3], D. Pokrajac[3]
[1]Department of Mechanical Engineering, Mappin Building, University of Sheffield, Sheffield, UK;
MS: mehdisedighi@gmail.com, SH: s.he@sheffield.ac.uk
[2]Division of Civil Engineering, University of Dundee, Dundee,UK; a.e.vardy@dundee.ac.uk
[3]School of Engineering, University of Aberdeen, Aberdeen,UK;
TOD: t.odonoghue@abdn.ac.uk, DP: d.pokrajac@abdn.ac.uk

ABSTRACT

A DNS study is performed to investigate turbulence in a steady-state channel flow at transitionally rough region ($k_s^+ = 8 - 41$) with a smooth top surface and a roughened bottom surface made of close-packed pyramids at several Reynolds numbers. Simulations in a channel with all smooth walls are also conducted to facilitate direct comparison. The skin friction factor results show an inflection point at $k_s^+ \approx 15$. Reynolds stress and normal vorticity show a similarity in the logarithmic region. In the outer layer, however, it appears that small- and large-scales structures exhibit different sensitivities to the existence of roughness. While the dissipation and vorticity, which are representing the small-scale structures, collapse to the corresponding smooth-wall values, Reynolds stress quantities containing great contributions of the large-scale structures do not exhibit this behaviour for $\frac{\delta}{k_t} = 20$ cases. The rough-case with $\frac{\delta}{k_t} = 40$, however, represents greater tendency to the similarity. Flow field patterns in the roughness sublayer demonstrate a significant dependence on Reynolds number. Also, at $y/k = 0.4$ above the crest, the flow structure of the case $Re_\tau = 670, k_s^+ = 41$ is very similar to that of $Re_\tau = 3520$, $\frac{\delta}{k_t} = 54.4$, $k_s^+ = 95$ in the experimental fully-rough results Hong et al. (2011).

INTRODUCTION

Although transitionally rough flow regime appears in many engineering applications such as wind turbine blades, atmospheric boundary layer and ship hulls, there are far fewer studies on flows in this regime than in the fully rough regime. In addition, most studies on rough-wall flows have used simple 2-D geometry (e.g. Krogstad et al. 2005; Coceal et al. 2007). In experimental studies with compact 3D roughness, the measurements are often limited to the region above the roughness crest due to experimental difficulties (e.g. Hong et al. 2011; Flack et al. 2012). A few exceptions include Talapatra and Katz (2012, 2013), who studied fully-rough channel flow using a microscopic holographic PIV.

In the present study, DNS is used to investigate steady-state channel flow in a transitionally rough regime with one smooth and one rough surface (referred to as rough-wall channel herein). The detailed flow behaviour in the regions below the roughness height, within the roughness sublayer and outer boundary layer are studied. Simulations of a smooth-wall channel flow are also carried out and the results are compared with those of corresponding rough-wall flows to examine the wall similarity hypothesis.

METHODOLOGY

DNS is performed using a revised version of an "in-house" code (Seddighi 2011; He and Seddighi 2013). The governing equations are written in dimensionless form normalised using the channel half height (H/2=δ) as the length scale, U_c(centreline laminar Poiseuille velocity) as the velocity scale, and ρU_c^2 for the pressure scale:

Momentum: $$\frac{\partial u_i}{\partial t} + u_j \frac{\partial u_i}{\partial x_j} = -\frac{\partial p}{\partial x_i} + \frac{1}{Re_c}\frac{\partial^2 u_i}{\partial x_j \partial x_j} + \Pi \qquad (1)$$

Conservation of mass: $$\frac{\partial u_i}{\partial x_i} = 0 \qquad (2)$$

The pressure gradient is split into two components, namely Π and $\frac{\partial p}{\partial x_i}$. The former is a spatially-uniform time-mean component of the streamwise pressure gradient required to balance the resistance due to friction and form drag (i.e. the values that would be needed to maintain a constant mass flow rate). The $\frac{\partial p}{\partial x_i}$component is a fluctuating component that varies both spatially and with time due to turbulence and flow heterogeneity.

A second order central finite difference method is used to discretize the spatial derivatives of the governing equations on a rectangular grid, where a three-dimensional staggered mesh is employed with a non-uniform spacing in the direction normal to the wall. For the time advancement, a low storage third-order Runge-Kutta scheme is used for the non-linear terms, and a second order Crank-Nicholson scheme is used for the viscous terms, which are combined with a fractional-step method described by Kim and Moin (1985) and Orlandi (2001). The Poisson equation for the pressure is solved by an efficient 2-D FFT Orlandi (2001). The roughness is treated using an immersed boundary method (IBM) described in detail by Orlandi and co-workers (e.g. Orlandi and Leonardi 2006; Leonardi et al. 2007; Leonardi and Orlandi 2008; Orlandi 2011). The

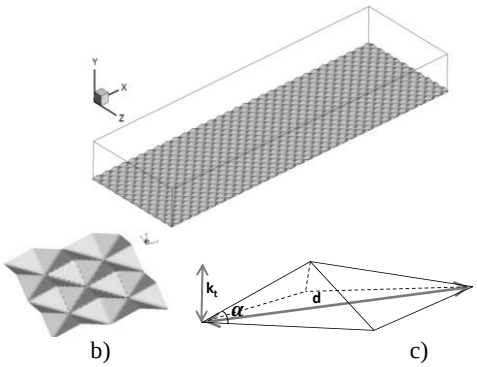

Figure 1. Geometry in the rough-wall simulations. a, geometry; b & c, Close-up view of the roughness topography and its parameters; $k_t = 0.05$, λ =d=0.3, $\alpha \approx 18.4$.

Table 1: Some details of the cases simulated.

Surface	Case	Re_b ≈	Re_τ ≈	k_t/δ	k^+	k_s^+	$\frac{\delta_t}{H/2}$
Smooth	S3500	3500	210	0	0	0	1
	S7400	7400	420	0	0	0	1
	S12600	12600	650	0	0	0	1
Rough	PA1500	1500	100	0.05	5.2	7.7	1.02
	PA2300	2300	150	0.05	8	12	1.03
	PA2800	2800	210	0.05	9.7	14.5	1.07
	PA3500	3500	265	0.05	12	18	1.08
	PA4200	4200	325	0.05	14	21.8	1.10
	PA4700	4700	470	0.05	16.5	24.8	1.13
	PA7400	7400	670	0.05	27.2	40.8	1.21
	PAB7400	7400	470	0.025	11.6	17.3	1.05

method is a revised IBM approach initially was developed by Fadlun et al. (2000).

In the rough-wall cases, a smooth top surface and a close-packed pyramids-roughened bottom surface are used (Figure 1). The slope angle of the lateral edge of the pyramid with the horizontal and the relative roughness are $\alpha \cong 18.4°$(9.5°for PAB7400-case) and $\frac{k_t}{H/2}$=0.05 (0.025 for PAB7400-case), respectively, where $k_t = k$ is peak-to-trough roughness height.

The computational domain in the streamwise and spanwise directions are 9.6(H/2), and 3(H/2), where H is the channel height. A total of 1024 and 480 mesh points over 32 and 10 pyramid wavelengths (with $\lambda_x = \lambda_z = \lambda =$ 0.3, Figure 1), are used in the streamwise (x) and spanwise (z) directions, respectively. In the wall-normal direction, a total number of 240 points is used, out of which 24 points (14 points for PAB7400-case) are equally spaced over the peak to trough roughness height, k_t. The periodicity was imposed for both the streamwise and spanwise directions and the no-slip condition was used for all rigid surfaces. The code is validated against well-known DNS benchmark data and shows close agreement (Seddighi 2011; Seddighi et al. 2011; He and Seddighi 2013).

RESULTS AND DISSCUSSION

Simulations of rough-wall channel flows have been carried out for 7 Reynolds numbers ranging from $Re_b =$ 1500 to $Re_b = 7400$, where $Re_b = \frac{H/2 \times U_b}{\upsilon}$, U_b is bulk velocity and H is the channel-height. Additionally, simulations of smooth-wall channel flow have been carried out for three Re_τ corresponding to the rough-wall cases PA2800, PA4700, and PA7400, in order to facilitate direct comparison. Details of simulation test-cases are presented in Table 1. Note that Re_τ is based on friction velocity u_τ and effective channel half-height (δ_t), defined by the location where the turbulent shear stress vanishes. For the rough-wall cases, the friction velocity of the lower (rough-wall) is used, but the average value of the upper and lower walls is used for the smooth-wall cases. δ_t coincides with the geometrical channel half-height (H/2) for the smooth-wall cases while it is slightly higher than H/2 for the rough-wall cases (Table 1). For each case, the DNS has first been run until the flow is fully developed. The simulation is then further continued in order to obtain around 50 independent flow realizations for ensemble averaging. The averaging has been done using two methods: i) A spatial followed by ensemble averaging denoted by angle brackets, < >. This method is the same as standard averaging in smooth-wall channel studies in which data are first spatially averaged over two homogeneous directions x and z and then ensemble averaged over the number of independent realisations. Consequently, around 1024×480×50≈25M data points are utilized for the statistical data presented at each y-location. This method is used for both smooth- and rough-wall cases. For smooth-cases, however, the data are further averaged over the upper and the lower walls of the channel, hereby doubling the number of samples for averaging. ii) Conditional averaging denoted by <~>: the data are spatially averaged over points located at the same position with respect to the pyramid wavelength and then, similar to (i), ensemble averaged over time. Accordingly, each conditionally-averaged result is obtained from 32×10×50=16K data points. This method is carried out for the rough-case in order to investigate spatial variability of turbulence quantities within a roughness wavelength.

Flow visualisations

Unlike typical experimental studies, DNS simulations can provide detailed information below the roughness crest. Figure 2 shows the conditionally-averaged streamwise velocity for one wavelength at several planes in the wall-normal direction, where $y = 0$ denotes the plane located at the roughness crest. It is seen that, for both low and high Reynolds number cases, the direct effect of roughness in modifying the flow pattern largely vanishes at $y = 2k$ above the crest. The location of the minimum velocity appears in the lee-side for the lowest Reynolds case, PA1500, but is shifted down to the face-side for PA7400. These regions are associated with high turbulent shear

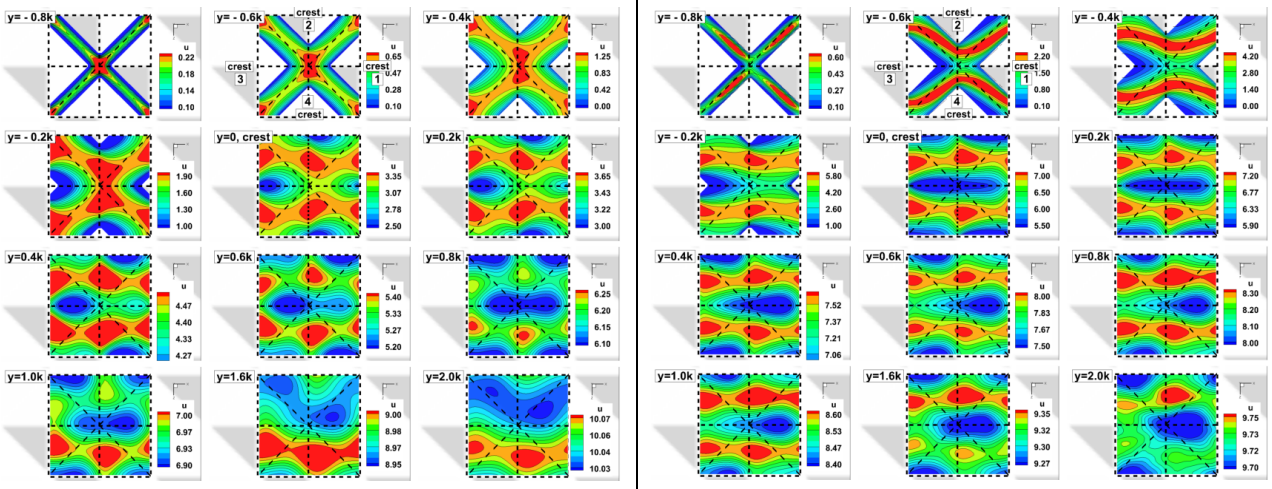

a) $Re_b = 1500$ b) $Re_b = 7400$

Figure 2. Conditionally-averaged streamwise velocity component at selected elevations relative to roughness crest.

stress (not shown here). The pattern exhibited for the y = 0.4k plane at $Re_b = 7400$ is strikingly similar to that seen in the fully rough regime case (Figure 8, Hong, Katz, & Schultz 2011). This, together with the roughness function profile and other results discussed in this paper, suggests that the flow behaviour in PA7400 is very similar to that of a fully-rough flow.

Skin friction factor and roughness function

The skin friction factor coefficient, c_f, is defined as:

$$c_f = \frac{\tau_w}{\frac{1}{2}\rho U_b^2} \quad (3)$$

The calculation of the wall shear stress for the smooth wall, τ_{ws}, is straightforward and is carried out in the same way as for the smooth-wall case through the following formula

$$\tau_{ws} = \mu \frac{\partial \langle u_1 \rangle}{\partial y}|_{y=y_w} \quad (4)$$

The bottom wall shear stress, however, is calculated using a method based on τ_{ws} and the total pressure drop of the channel (Π) (Leonardi et al. 2005; Seddighi 2011). Figure 3 shows the variation of c_f versus Reynolds number for the rough-cases investigated. Also shown for comparison are some results for smooth-wall channels from the literature (Dean 1978; Zanoun et al. 2003; Monty 2005; Flack et al. 2012) and results of Flack et al. (2012) for a 220-grit sandpaper ($\frac{k_t}{\delta_t} \cong 0.03$). The present results for smooth-wall agree well with those obtained by Flack et al. (2012). They are, however, noticeably higher than those of Zanoun et al. (2003), and slightly lower than the experimental data of Monty (2005). The skin friction coefficient for the rough-wall appears to exhibit the inflectional behaviour of Nikuradse transitional rough data rather than the monotonic Colebrook' relation (Colebrook 1939). This trend, which is similar (but with different values and minima) to Flack's 220-grid sandpaper data, has also been demonstrated in some other transitional rough wall studies (Allen et al. 2005; Allen et al. 2007; Langelandsvik et al. 2008; Flack et al. 2012).

It is well-established that the value of the roughness function, ΔU^+, is a measure of momentum loss and is directly related to the increase in overall friction due to the existence of roughness (see for example Flack and Schultz 2010). ΔU^+ is often plotted against the equivalent roughness height k_s^+ to show how well data of various roughness type in the fully-rough flow correlate. Such a plot of ΔU^+ against k_s^+ is shown in Figure 4. Also shown in the plot are the Nikuradse data and the experimental results of Schultz and Flack (2009), who studied a rough-wall

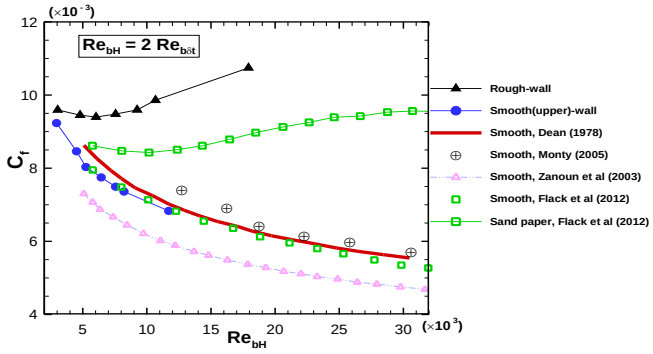

Figure 3. Skin friction coefficient versus Reynolds number.

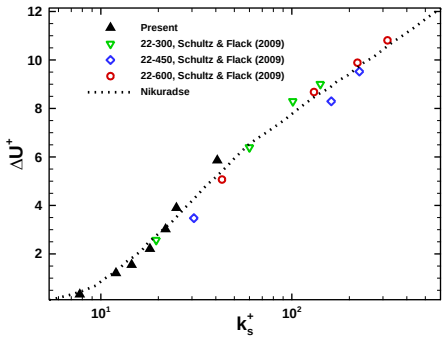

Figure 4. Roughness function versus equivalent roughness height.

boundary layer with similar roughness. The results are in reasonable agreement, which suggest that, consistent with the findings of Schultz and Myers (2003), ΔU^+ for a given roughness geometry is similar in a boundary layer flow, pipe flow or a channel flow. Note that, the equivalent roughness height, k_s, is related to the roughness height through k_s ~1.5 k_t. This was obtained by applying the results of the highest Reynolds number (PA7400) to the following formula for fully-rough flow (see for example eq. 1.3 in Krogstad et al. 2005):

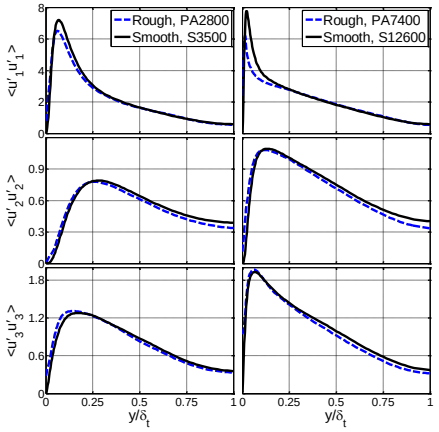

Figure 5. Normal stress profiles.

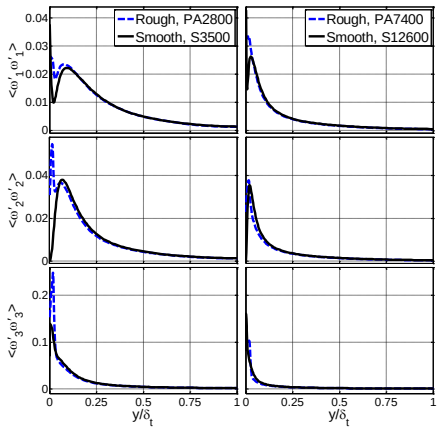

Figure 6. Profiles of mean square vorticity.

$$\Delta U^+ = \frac{1}{\kappa}\ln k_s^+ + B - C \qquad (5)$$

where, κ is the von Karman constant, B is the smooth-wall log-law intercept (κ = 0.4 and B = 5.39 for PA7400), and C is skin friction coefficient which is $C \cong 8.5$ for the fully-rough flow. The above equivalent roughness height ratio, which is in agreement with studies on fully-rough pyramid geometry (Schultz and Flack 2009; Hong et al. 2011; Hong et al. 2012), is then applied to all rough cases studied.

Wall Similarity

The classical theory for turbulent flows over rough walls is based on the Reynolds number similarity concept of Townsend (1976) which was extended as wall similarity by Perry and Abell (1977). This hypothesis, which has been investigated extensively over the last three decades, indicates that the direct influence of roughness is confined to a region of several-roughness heights above the surface, namely the roughness sublayer, and that all flow statistics in the outer layer are unaffected by the wall roughness. In most studies with available flow field (DNS/PIV), the height of the roughness sublayer is normally defined as the distance at which spatial variation of Reynolds stresses is diminished (Bhaganagar et al. 2004; Hong et al. 2011; Lee et al. 2011). This sublayer has been found to be 2-5 times the roughness height. Another definition of the roughness sublayer thickness is the distance beyond which the statistical values of rough- and smooth-wall start to collapse (Bakken et al. 2005; Schultz and Flack 2005). In the present results (Figure 2) the spatial variation of turbulence quantities become negligible above y/k~2 and so this height, which is almost independent of Reynolds number, is taken as the roughness sublayer. The present results show very good wall similarity for the mean velocity (not shown here) for all Reynolds numbers investigated.

Figures 5 and 6 show the normal stresses and the correlations of the vorticity fluctuations plotted against y/δ_t for PA2800 and PA7400. It is seen that the streamwise normal stress, $\langle u'_1 u'_1 \rangle$, exhibits excellent wall similarity (Figure 5-top), whereas the wall-normal and spanwise components of the rough-cases show a reduction in comparison with the corresponding smooth-cases values, beyond $y/\delta_t \approx 0.25$. Another point to be noted is the reduction caused by the roughness (greater at the higher Reynolds case) for $\langle u'_1 u'_1 \rangle$ in the $y/\delta_t \sim < 0.2$ or $y/k_t \sim < 4$ region, while a slight increase is seen in the other two components. This shows the effect of an increase in isotropy due to the roughness, which is discussed in the next section. In contrast to the normal stress behaviour, the normal mean square vorticity shows good similarity beyond $y/\delta_t \approx 0.1$ for both cases. The Reynolds stresses are generally representative of the large-scale structures, while the small-scale behaviour can be associated with quantities involving velocity derivatives, such as the vorticity, dissipation, etc. The above results show that the

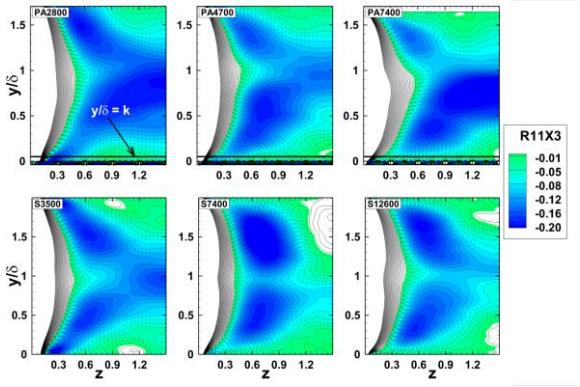

Figure 7. Two-point spanwise correlation contours of streamwise velocity, comparison between smooth- & rough- cases.

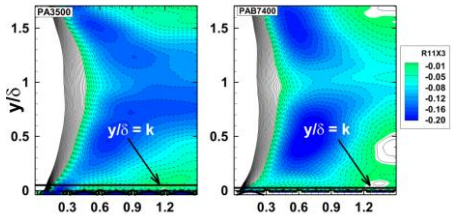

Figure 8. Two-point spanwise correlation contours of streamwise velocity at similar $k_s^+ \approx 18$, PA3500 & PAB7400.

wall similarity between rough- and smooth-data is present in the small-scale structures in the outer layer, but the large-scale structures show less similarity.

To further examine quantitative influence of the roughness on the large-scales, contour plots of spanwise two-point auto-correlations of streamwise velocity component for three pairs of rough- and corresponding smooth-cases are shown in Figure 7. The region with negative values are shaded. The mean spacing between the streaks (streaky structures exist in flows which are typical of low Reynolds number turbulent flows) can be approximated by two times the distance at which the minimum value of the streamwise component occurs. The spacing of the streaks just above the wall (y/δ~0.1) in the S3500 smooth-case centred at around z ≈ 2 × 0.26, which corresponds to $z^+ \approx 2 \times 55$, is in agreement with the results of Kim et al. (1987), who obtained a value of 100 for the spacing at $y^+ \cong 10.52$ for $Re_\tau = 180$. Such near streaks become very weak at higher Reynolds numbers. In the rough-wall cases, the structure of the flow is clearly not symmetric – the flow on the top (smooth) wall is very different from that on the bottom (rough) wall. Comparing with the smooth-cases, the difference is smaller at low-Reynolds number, but becomes greater at $Re_b = 7400$. It is seen that the structures of the flow are very different in the rough-wall and smooth-wall cases, which explains the differences seen in the normal stresses in Figure 5. Figure 8 shows the spanwise correlations for two cases PA3500 and PAB7400, which have similar $k_s^+ \approx 18$, but different roughness height (k/δ =0.05 and 0.025 respectively). While the contour of PA3500 is grossly similar to those seen for the rough cases shown in Figure 7, the pattern of the PAB7400 is significantly different. The high-intensity negative region seen in the central region in the cases with k/δ =0.05 is no longer exhibited in the PAB7400 case. The structure in this case is rather similar to the pattern of the smooth-case S7400. The better similarity of the case with $\frac{\delta}{k_t} = 40$ supports the minimum similarity blockage ratio of 40 proposed by Jiménez (2004).

Anisotropy

Turbulence anisotropy can be examined by studying the Reynolds stress anisotropy tensor (b_{ij}), the vorticity (v_{ij}) and dissipation (d_{ij}) anisotropy tensors. The former (b_{ij}) mainly represents the contribution of large scale structures. The latter two quantities have greater weighting of the high-wave number structures and are normally used to study the small-scale structure anisotropy (Lumley 1978; Kida and Hunt 1989; Antonia et al. 1991; Shafi and Antonia 1997; Djenidi and Tardu 2012). They are defined as:

$$b_{ij} = \frac{\langle u'_i u'_j \rangle}{\langle u'_i u'_i \rangle} - \frac{\delta_{ij}}{3},\ v_{ij} = \frac{\langle \omega'_i \omega'_j \rangle}{\langle \omega'_i \omega'_i \rangle} - \frac{\delta_{ij}}{3},\ d_{ij} = \frac{\langle \varepsilon'_i \varepsilon'_j \rangle}{\langle \varepsilon'_i \varepsilon'_i \rangle} - \frac{\delta_{ij}}{3} \quad (6)$$

where, δ_{ij} is the Kronecker delta tensor, and ω and ε are vorticity and dissipation rate, respectively. Studying such parameters in the rough-wall not only provides information on sensitivity of different length-scales structures to the presence of roughness, but also is useful in developing turbulence modelling. Also, since these normalised parameters are no longer dependent on the friction velocity, they could be of interest in experimental studies where determining the friction velocity is an issue.

One way of examining the overal anisotropy is via the invariant function, $F = 27III + 9II + 1$, proposed by Lumley (1978) where -II= $\frac{\varphi_{ij}\varphi_{ji}}{2}$ and III= $\frac{\varphi_{ij}\varphi_{jk}\varphi_{ki}}{3}$ are respectively, second and third principal invariant tensors (φ_{ij} denotes b_{ij}, v_{ij}or d_{ij}). F=0 denotes two-component turbulence while F=1 indicates the isotropic state. In a smooth channel with no transpiration, the wall-normal velocity must be zero at the wall and this two-dimensional turbulence state leads to F=0. Moving away from the wall and toward the centreline, F increases and approches 1, which indicates an isotropic state. Figure 9 shows the variation of Reynolds stress invariant function, F_b, in the outer scales for the three rough cases PA2800, PA4700 and PA7400, and the three corresponding smooth cases together with the case simulated at the lowest Reynolds number, PA1500. Also shown in the figure are the results of a 2-d k-type rib roughness of Krogstad et al. (2005) (denoted by RIB400 and RIB600 for the cases at Re_τ = 400 and 600, respectively). There are several trends that can be seen from this figure. i) The anisotropy in the region

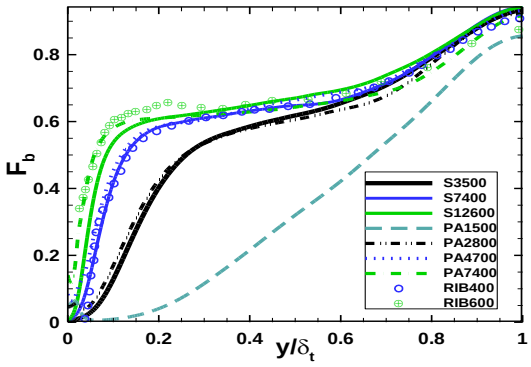

Figure 9. Invariant function of Reynolds stresses.

very close to the roughness is slightly smaller than that in the corresponding smooth-wall case. This supports observations for many studies showing roughness improves the isotropy. ii) Beyond $\frac{y}{\delta_t} \approx 0.2$ a noticeable increase in the anisotropy is seen. This is in contrast with some other studies, which show improvement of anisotropy in the outer layer (Shafi and Antonia 1995; Djenidi et al. 1999; Antonia and Krogstad 2001; Smalley et al. 2002; Roussinova et al. 2009), or some others, which show wall similarity (Krogstad et al. 2005; Ashrafian and Andersson 2006; Lee and Sung 2007; Busse and Sandham 2012) for Reynolds stress anisotropy. However, the present results (in particular for PA7400), support the observation of Leonardi et al. (2006) who performed DNS simulation for rib roughness with $\frac{k}{\delta} = 0.1$ at several pitch to height ratios of $\frac{w}{k}$ = 1,3,7 and 59. Their results for $\frac{w}{k} = 7$ exhibit a reduction of anisotropy in the region close to the crest and an increase in the outer layer ($\frac{y}{\delta} > 0.2$), in comparision with the smooth-wall data. According to these observations, it appears that the effect of roughness on the Reynolds stress anisotropy depends on the flow type and roughness geometry. The dissipation and vorticity invariant functions and Anisotropy Invariant Map, AIM (not shown here), on

the other hand, exhibit a good agreement over the smooth- and rough-wall cases in this region, which confirms that the small-scale structures exhibit stronger wall similarity. iii) The invariant function remains almost the same ($F_b \approx 0.6$) throughout the logarithmic region. It is specially evident for the highest Reynolds number case PA7400, which has the most extended logarithmic region among the cases. The results of a 2-d k-type rib roughness at $Re_\tau = 400$ and 600 reproduced from Krogstad et al. (2005), which are also shown, demonstrate the same F_b-constant trend in the log-layer. iv) Similar to the smooth-wall, a clear Reynolds number effect (stronger toward the centre) on the anisotropy can be seen.

CONCLUSION

Transitional rough flow over a 3-d pyramid roughness is investigated using DNS of channel flow with a bottom wall made of close-packed roughness and a smooth top wall. Results indicate that the small-scale structures show wall similarity, even for transitional flow with high relative roughness. For the large-scale structures, on the other hand, good agreement between the smooth and rough wall values has been observed for the cases with high blockage ratio, $\frac{\delta}{k_t} = 40$, but not for the case of $\frac{\delta}{k_t} = 20$. The Reynolds stress anisotropy invariant function and spanwise two-point correlations confirm the differences seen in the normal stresses. The presence of the roughness does not change the anisotropy in the log-law region but reduces it close to the wall. In the outer layer, however, the roughness of $\frac{\delta}{k_t} = 20$ increases the isotropy in the roughness sublayer but reduces it in the region beyond the log-law (in the outer layer). The flow pattern in the roughness sublayer changes significantly with increasing Reynolds number. The flow structure at $y/k = 0.4$ above the crest for the case PA7400 ($Re_\tau = 670, k_s^+ = 41$) is very similar to that observed experimentally for the fully-rough case with $Re_\tau = 3520$, $\frac{\delta}{k_t} = 54.4,\ k_s^+ = 95$.

REFERENCES

ALLEN, J. J., SHOCKLING, M. A., KUNKEL, G. J. & SMITS, A. J. 2007. Turbulent flow in smooth and rough pipes. *Philosophical Transactions of the Royal Society A: Mathematical, Physical and Engineering Sciences,* 365**,** 699-714.

ALLEN, J. J., SHOCKLING, M. A. & SMITS, A. J. 2005. Evaluation of a universal transitional resistance diagram for pipes with honed surfaces. *Physics of Fluids,* 17**,** 1-4.

ANTONIA, R. A., KIM, J. & BROWNE, L. W. B. 1991. Some characteristics of small-scale turbulence in a turbulent duct flow. *Journal of Fluid Mechanics,* 233**,** 369-388.

ANTONIA, R. A. & KROGSTAD, P. Å. 2001. Turbulence structure in boundary layers over different types of surface roughness. *Fluid Dynamics Research,* 28**,** 139-157.

ASHRAFIAN, A. & ANDERSSON, H. I. 2006. The structure of turbulence in a rod-roughened channel. *International Journal of Heat and Fluid Flow,* 27**,** 65-79.

BAKKEN, O. M., KROGSTAD, P. Å., ASHRAFIAN, A. & ANDERSSON, H. I. 2005. Reynolds number effects in the outer layer of the turbulent flow in a channel with rough walls. *Physics of Fluids,* 17**,** 1-16.

BHAGANAGAR, K., KIM, J. & COLEMAN, G. 2004. Effect of roughness on wall-bounded turbulence. *Flow, Turbulence and Combustion,* 72**,** 463-492.

BUSSE, A. & SANDHAM, N. D. 2012. Parametric forcing approach to rough-wall turbulent channel flow. *Journal of Fluid Mechanics,* 712**,** 169-202.

COCEAL, O., DOBRE, A., THOMAS, T. G. & BELCHER, S. E. 2007. Structure of turbulent flow over regular arrays of cubical roughness. *Journal of Fluid Mechanics,* 589**,** 375-409.

COLEBROOK, C. F. 1939. Turbulent flow in pipes with particular reference to the transition region between the smooth and rough pipe laws. *J. Inst. Civ. Eng.,* 11**,** 133-156.

DEAN, R. B. 1978. Reynolds number dependence of skin friction and other bulk flow variables in two-dimensional rectangular duct flow. *Journal of Fluids Engineering, Transactions of the ASME,* 100**,** 215-223.

DJENIDI, L., ELAVARASAN, R. & ANTONIA, R. A. 1999. The turbulent boundary layer over transverse square cavities. *Journal of Fluid Mechanics,* 395**,** 271-294.

DJENIDI, L. & TARDU, S. F. 2012. On the anisotropy of a low-Reynolds-number grid turbulence. *Journal of Fluid Mechanics,* 702**,** 332-353.

FADLUN, E. A., VERZICCO, R., ORLANDI, P. & MOHD-YUSOF, J. 2000. Combined Immersed-Boundary Finite-Difference Methods for Three-Dimensional Complex Flow Simulations. *Journal of Computational Physics,* 161**,** 35-60.

FLACK, K. A. & SCHULTZ, M. P. 2010. Review of hydraulic roughness scales in the fully rough regime. *Journal of Fluids Engineering, Transactions of the ASME,* 132**,** 0412031-04120310.

FLACK, K. A., SCHULTZ, M. P. & ROSE, W. B. 2012. The onset of roughness effects in the transitionally rough regime. *International Journal of Heat and Fluid Flow,* 35**,** 160-167.

HE, S. & SEDDIGHI, M. 2013. Turbulence in transient channel flow. *Journal of Fluid Mechanics,* 715**,** 60-102.

HONG, J., KATZ, J., MENEVEAU, C. & SCHULTZ, M. P. 2012. Coherent structures and associated subgrid-scale energy transfer in a rough-wall turbulent channel flow. *Journal of Fluid Mechanics,* 1-37.

HONG, J., KATZ, J. & SCHULTZ, M. P. 2011. Near-wall turbulence statistics and flow structures over three-dimensional roughness in a turbulent channel flow. *Journal of Fluid Mechanics,* 667**,** 1-37.

JIMÉNEZ, J. 2004. Turbulent flows over rough walls. *Annual Review of Fluid Mechanics,* 36**,** 173-196.

KIDA, S. & HUNT, J. C. R. 1989. Interaction between different scales of turbulence over short times. *Journal of Fluid Mechanics,* 201**,** 411-445.

KIM, J. & MOIN, P. 1985. Application of a fractional-step method to incompressible Navier-Stokes equations. *Journal of Computational Physics,* 59**,** 308-323.

KIM, J., MOIN, P. & MOSER, R. 1987. Turbulence statistics in fully developed channel flow at low Reynolds number. *Journal of Fluid Mechanics,* 177**,** 133-166.

KROGSTAD, P. Å., ANDERSSON, H. I., BAKKEN, O. M. & ASHRAFIAN, A. 2005. An experimental and numerical study of channel flow with rough walls. *Journal of Fluid Mechanics,* 530**,** 327-352.

LANGELANDSVIK, L. I., KUNKEL, G. J. & SMITS, A. J. 2008. Flow in a commercial steel pipe. *Journal of Fluid Mechanics,* 595**,** 323-339.

LEE, J. H., SUNG, H. J. & KROGSTAD, P. A. 2011. Direct numerical simulation of the turbulent boundary layer over a cube-roughened wall. *Journal of Fluid Mechanics,* 669**,** 397-431.

LEE, S. H. & SUNG, H. J. 2007. Direct numerical simulation of the turbulent boundary layer over a rod-roughened wall. *Journal of Fluid Mechanics,* 584**,** 125-146.

LEONARDI, S. & ORLANDI, P. 2008. *RE: A numerical method for turbulent flows over complex geometry.*

LEONARDI, S., ORLANDI, P. & ANTONIA, R. A. 2005. A method for determining the frictional velocity in a turbulent channel flow with roughness on the bottom wall. *Experiments in Fluids,* 38**,** 796-800.

LEONARDI, S., ORLANDI, P. & ANTONIA, R. A. 2007. Properties of d- and k-type roughness in a turbulent channel flow. *Physics of Fluids,* 19.

LEONARDI, S., ORLANDI, P., DJENIDI, L. & ANTONIA, R. 2006. Guidelines for Modeling a 2D Rough Wall Channel Flow. *Flow, Turbulence and Combustion,* 77**,** 41-57.

LUMLEY, J. L. 1978. Computational modeling of turbulent flows. *Advances in Applied Mechanics,* 18**,** 123-176.

MONTY, J. P. 2005. *Developments in smooth wall turbulent duct flows.* PhD Thesis, The University of Melbourne.

ORLANDI, P. 2001. *Fluid flow phenomena: a numerical toolkit,* Kluwer.

ORLANDI, P. 2011. DNS of transitional rough channels. *Journal of Turbulence,* 12**,** 1-20.

ORLANDI, P. & LEONARDI, S. 2006. DNS of turbulent channel flows with two- and three-dimensional roughness. *Journal of Turbulence,* 7**,** 1-22.

PERRY, A. E. & ABELL, C. J. 1977. Asymptotic similarity of turbulence structures in smooth and rough walled pipes. *Journal of Fluid Mechanics,* 79**,** 785799.

ROUSSINOVA, V., BALACHANDAR, R. & BISWAS, N. 2009. Reynolds stress anisotropy in open-channel flow. *Journal of Hydraulic Engineering,* 135**,** 812-824.

SCHULTZ, M. P. & FLACK, K. A. 2005. Outer layer similarity in fully rough turbulent boundary layers. *Experiments in Fluids,* 38**,** 328-340.

SCHULTZ, M. P. & FLACK, K. A. 2009. Turbulent boundary layers on a systematically varied rough wall. *Physics of Fluids,* 21.

SEDDIGHI, M. 2011. *Study of turbulence and wall shear stress in unsteady flow over smooth and rough wall surfaces.* Ph.D, University of Aberdeen.

SEDDIGHI, M., HE, S., ORLANDI, P. & VARDY, A. E. 2011. A comparative study of turbulence in ramp-up and ramp-down unsteady flows. *Flow, Turbulence and Combustion,* 86**,** 439-454.

SHAFI, H. S. & ANTONIA, R. A. 1995. Anisotropy of the Reynolds stresses in a turbulent boundary layer on a rough wall. *Experiments in Fluids,* 18**,** 213-215.

SHAFI, H. S. & ANTONIA, R. A. 1997. Small-scale characteristics of a turbulent boundary layer over a rough wall. *Journal of Fluid Mechanics,* 342**,** 263-293.

SMALLEY, R., LEONARDI, S., ANTONIA, R., DJENIDI, L. & ORLANDI, P. 2002. Reynolds stress anisotropy of turbulent rough wall layers. *Experiments in Fluids,* 33**,** 31-37.

TALAPATRA, S. & KATZ, J. 2012. Coherent structures in the inner part of a rough-wall channel flow resolved using holographic PIV. *Journal of Fluid Mechanics,* 711**,** 161-170.

TALAPATRA, S. & KATZ, J. 2013. Three-dimensional velocity measurements in a roughness sublayer using microscopic digital in-line holography and optical index matching. *Measurement Science and Technology,* 24.

TOWNSEND, A. A. 1976. *The structure of turbulent shear flow,* Cambridge University Press.

ZANOUN, E. S., DURST, F. & NAGIB, H. 2003. Evaluating the law of the wall in two-dimensional fully developed turbulent channel flows. *Physics of Fluids,* 15**,** 3079-3089.